

Spin waves and magnetic interactions in LiCu_2O_2 T. Masuda,¹ A. Zheludev,¹ B. Roessli,² A. Bush,³ M. Markina,⁴ and A. Vasiliev⁴¹Condensed Matter Sciences Division, Oak Ridge National Laboratory, Oak Ridge, Tennessee 37831-6393, USA²Laboratory for Neutron Scattering, ETH Zurich and Paul Scherrer Institute, CH-5232 Villigen PSI, Switzerland³Moscow Institute of Radiotechnics, Electronics and Automation, Moscow 117464, Russia⁴Low Temperature Physics Department, Moscow State University, Moscow 119992, Russia

(Received 21 December 2004; published 1 July 2005)

The quasi-one-dimensional helimagnet LiCu_2O_2 was studied by single crystal inelastic neutron scattering. The dispersion relation of spin wave excitations was measured in the vicinity of the principal magnetic Bragg reflection. A spin wave theoretical analysis of the data yields an estimate of the relevant exchange constants and explains the mechanism of geometric frustration that leads to helimagnetism. It is found that the simple antiferromagnetic J_1 - J_2 model that was previously proposed is inadequate for LiCu_2O_2 . The experimental findings are generally in a qualitative agreement with first principles calculations of [A. A. Gippius, E. N. Morozova, A. S. Moskvina, A. V. Zalesky, A. A. Bush, M. Baenitz, H. Rosner, and S.-L. Drechsler, Phys. Rev. B **70**, 020406 (2004)], though certain important discrepancies remain to be explained.

DOI: 10.1103/PhysRevB.72.014405

PACS number(s): 75.50.-y, 75.30.Ds, 75.30.Et, 75.25.+z

I. INTRODUCTION

LiCu_2O_2 is a quasi-one-dimensional magnetic material that has recently attracted a great deal of attention.¹⁻⁴ Muon spin resonance,⁵ neutron scattering experiments,⁶ and NMR studies⁷ clearly demonstrated that this $S=1/2$ system has an incommensurate helimagnetic ground state. In our previous work⁶ we postulated a simple model of magnetic interactions that seemed to account well for the observed properties. It was proposed that LiCu_2O_2 features weakly coupled zigzag $S=1/2$ chain with competing nearest-neighbor J_1 and next-nearest-neighbor J_2 antiferromagnetic interactions. Due to geometric frustration this model exhibits an unusual competition between a quantum-disordered gapped⁹ ground state with commensurate spin correlations,¹⁰ and semiclassical helimagnetic incommensurate state. However, independent first-principles numerical studies^{7,11} suggested a totally different model for the geometric frustration in LiCu_2O_2 . According to that work, the nearest-neighbor J_1 interactions are actually ferromagnetic, and it is the unusually large fourth-nearest-neighbor antiferromagnetic coupling constant J_4 that causes geometric frustration and favors helimagnetism. A similar scenario was recently proposed for a very similar isostructural helimagnet NaCu_2O_2 .¹²

Bulk magnetic susceptibility data for LiCu_2O_2 seem to be compatible with both models,^{6,11} and are thus inconclusive. The only direct way to determine (effective) exchange constants is by means of single crystal inelastic neutron spectroscopy. This technique can probe the dispersion relation of spin wave excitations in the system. In the present paper we describe the results of such a study. Preliminary results were reported in Ref. 8. We find that the actual topology of magnetic coupling is indeed more complex than originally envisioned.

A. Structural considerations

LiCu_2O_2 has a layered charge-ordered orthorhombic crystal structure [space group $Pnma$, $a=5.730(1)$ Å, b

$=2.8606(4)$ Å, and $c=12.417(2)$ Å], as described in detail in Refs. 3 and 5. The magnetism is due to double chains of Cu^{2+} ions that run along the crystallographic b axis. The period of each “leg” of the double spin chains is equal to b . The two legs are offset by the $b/2$ relative to each other and thus form a “triangular ladder,” as illustrated in Fig. 1(a). These double chains are arranged in layers parallel to the (a, b) plane and are effectively separated along the c direction by planes of non-magnetic Cu^+ ions.

The approximate magnetic structure was determined in Ref. 6 and is illustrated in Fig. 1 of that paper. The ordering

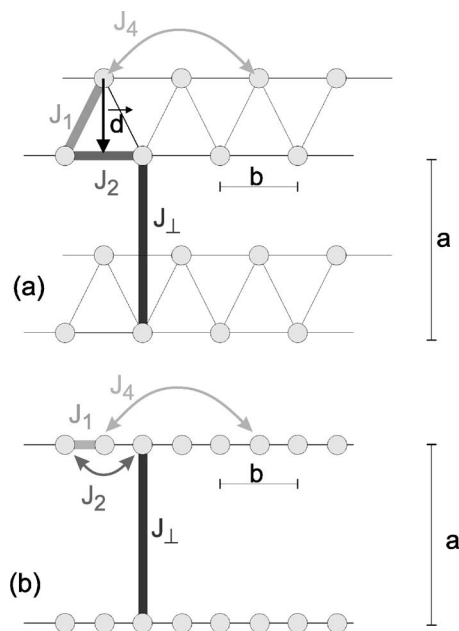


FIG. 1. (a) A schematic view of exchange interactions between magnetic Cu^{2+} ions in LiCu_2O_2 . (b) An equivalent Bravais lattice of spins obtained by displacing every other Cu^{2+} ion in the original non-Bravais lattice by the vector \mathbf{d} . It is assumed that the spin Hamiltonian remains intact upon this transformation.

temperature is $T_c=24$ K. Each double spin chain carries a planar helix of spins. The magnetic propagation vector is $\mathbf{q}_0=(0.5, \zeta, 0)$ with $\zeta \approx 0.827$. Consecutive spins on each rung are almost parallel, being rotated relative to each other by an angle $\phi=2\pi\zeta$. Within each double chain any nearest-neighbor spins from opposite legs are almost antiparallel and form an angle $\phi/2=\pi\zeta$. Preliminary neutron diffraction experiments were consistent with (a, b) being the spin rotation plane, but independent NMR studies clearly show an out-of-plane component.⁷ This suggests that the spin rotation planes are, in fact, tilted relative to a high-symmetry orientation. The issue deserves further investigation, perhaps involving more accurate diffraction measurements. However, if magnetic anisotropy effects are negligible compared to Heisenberg exchange interactions (a reasonable assumption for Cu^{2+} ions), the actual arrangement of spin rotation planes should not affect spin wave dispersion relations that are the focus of the present study.

The main goal of the inelastic neutron scattering experiments described below is to establish the hierarchy of exchange interactions. The corresponding coupling constants are schematically shown in Fig. 1(a), and define a model Heisenberg Hamiltonian for LiCu_2O_2

$$\tilde{H} = \sum_{i,j} [J_1 \mathbf{S}_{i,j} \mathbf{S}_{i+1,j} + J_2 \mathbf{S}_{i,j} \mathbf{S}_{i+2,j} + J_4 \mathbf{S}_{i,j} \mathbf{S}_{i+4,j} + J_{\perp} \mathbf{S}_{i,j} \mathbf{S}_{i,j+1}], \quad (1)$$

where the index i labels consecutive spins in each double chain, as shown in Fig. 1(a), and j labels the double chains.⁸

II. EXPERIMENT

In the present study we employed a 5 g single-crystal sample of LiCu_2O_2 . Crystal mosaic was not particularly good: irregular, with as much as a 4° full width at half maximum (FWHM) spread. This circumstance imposed certain constraints as will be discussed below. The measurements were carried out in two separate series of experiments. Neutrons with a fixed final energy of $E_f=13.5$ meV were used at the HB-1 thermal three-axis spectrometer at the High Flux Isotope Reactor at Oak Ridge National Laboratory, Oak Ridge, TN (ORNL) (Setup 1). Pyrolytic graphite PG (002) reflections were used for a monochromator and an analyzer. A PG filter was installed after the sample to eliminate higher-order beam contamination. The setup employed $48'-80'-80'-240$ collimators. Alternatively, we utilized cold neutrons with a final energy fixed at $E_f=5$ meV at the TASP three-axis instrument installed at the SINQ spallation source, Villigen PSI, Switzerland (Setup 2). A PG monochromator and analyzer were used with no additional collimation and a cold Be filter positioned after the sample. In all cases the sample was mounted with the (a, b) plane coinciding with the horizontal scattering plane of the instrument. The sample environment was a standard ‘‘Orange’’-type flow cryostat. Most of the data were taken at $T=1.5$ K.

Data collection procedures were aimed at minimizing the adverse effects of the broad mosaic spread of the sample. A large mosaic translated to a poor wave vector resolution per-

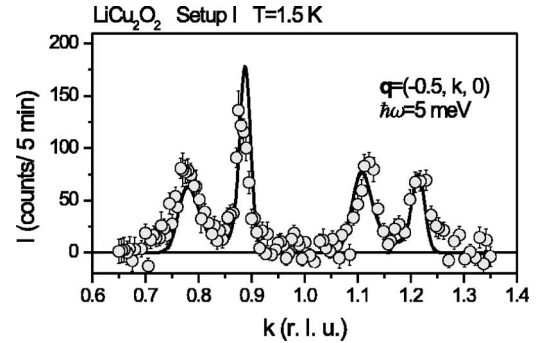


FIG. 2. A constant- E scan along the $(-0.5, k, 0)$ reciprocal-space rod measured in LiCu_2O_2 at $T=1.5$ K at an energy transfer of 5 meV (symbols) using Setup 1. The lines are a simulation based on the measured spin wave dispersion relation and the known resolution function of the instrument.

pendicular to the momentum transfer \mathbf{q} . Since the spin wave dispersion is steepest along b^* , the best focusing conditions are obtained for \mathbf{q} pointing close to that direction. Considering the intensity reduction due to the effect of magnetic form factors at large $|q|$, an optimal ‘‘window’’ for low-energy spin wave measurements was identified in the vicinity of the $(0.5, 0.827, 0)$ and $(0.5, 1.173, 0)$ magnetic Bragg peaks. Another advantage of this reciprocal-space region is that it is relatively clear of spurious scattering and phonons, that were carefully checked for. Most scans were repeated at $T=75$ K, i.e., well above T_c , to verify that the signal observed at low temperature is indeed of magnetic origin. In some cases smoothed high-temperature scans were used as background for point-by-point subtraction from the corresponding low-temperature data sets.

Another important technical problem that had to be dealt with is crystal twinning. In LiCu_2O_2 twinning occurs at a microscopic level.³ The a axis of one type of domain coincides with the b axis of the other domain type, since $a \approx 2b$. The immediate consequence is that neutron diffraction and inelastic scattering necessarily detect a joint signal originating from both domain types. As will be discussed in detail below, the contributions from different domains and different spin wave branches within each domain could be reliably separated only in the direct proximity of the $(0.5, 0.827, 0)$ and $(0.5, 1.173, 0)$ peaks. Even so, twinning reduces the effective sample volume by a factor of two. To avoid any confusion we will use the indexes h, k , and l to label wave vector components in the coordinate system defined by the reciprocal lattice of one particular domain type (type A). Indexes $h_B=2k$, $k_B=h/2$, and $l_B=l$ will refer to the other crystallographic domain (type B).

III. RESULTS

A typical constant-energy scan collected using Setup 1 is shown in Fig. 2. The non-magnetic background for this scan (featureless and typically about 80 counts per 5 min) was measured at $T=75$ K. A linear fit to the measured background was subtracted from the data shown. The four prominent peaks seen in this scan can be attributed to an acoustic

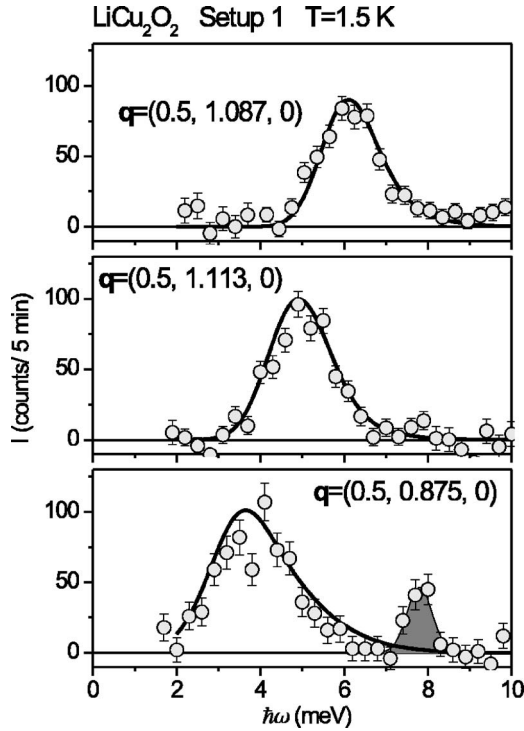


FIG. 3. Typical constant- q scans measured in LiCu_2O_2 (symbols) at $T=1.5$ K. The lines are as in Fig. 2. The shaded area in the lower scan is an “accidental Bragg” spurious peak originating from $2k_i$ scattering in the monochromator, $(0, 2, 0)$ Bragg scattering in the sample, and inelastic thermal-diffuse scattering in the analyzer. The spurious peak appears much narrower than the experimental resolution (about 2 meV FWHM).

spin wave emanating from two magnetic Bragg peaks at $(0.5, 0.827, 0)$ and $(0.5, 1.173, 0)$. Representative constant- q scans collected using the same setup are shown in Fig. 3, where a flat background has been subtracted from the data. All inelastic peaks observed for $0.75 \leq k \leq 1.25$ and $\hbar\omega \leq 8$ meV can be associated with a single branch of excitations. The corresponding dispersion relation along the crystallographic b axis was extracted from the measured scans using Gaussian fits. The result is plotted in circles in Fig. 4(a), where solid and open symbols indicate constant- q and constant- E measurements, respectively. Any attempts to follow the observed spin wave branch to higher energies were not successful. The mode’s intensity drops progressively, while the background increases and becomes structured. As will be explained below, part of this problem may be due to a multitude of additional spin wave branches from both types of domains. The situation was further aggravated by limited resolution, phonon scattering, and instrument-related spurious peaks. For this reason, throughout this paper we shall limit the discussion to experimental data collected at low energies in direct proximity of the two above-mentioned magnetic Bragg peaks.

Additional measurements were performed using Setup 2 to determine the dispersion along the a^* axis. Typical scans and the measured dispersion curve are shown in Figs. 5 and 4(b), respectively. The important zone-boundary scan at $(0, 0.827, 0)$ was also measured using Setup 1 in the range

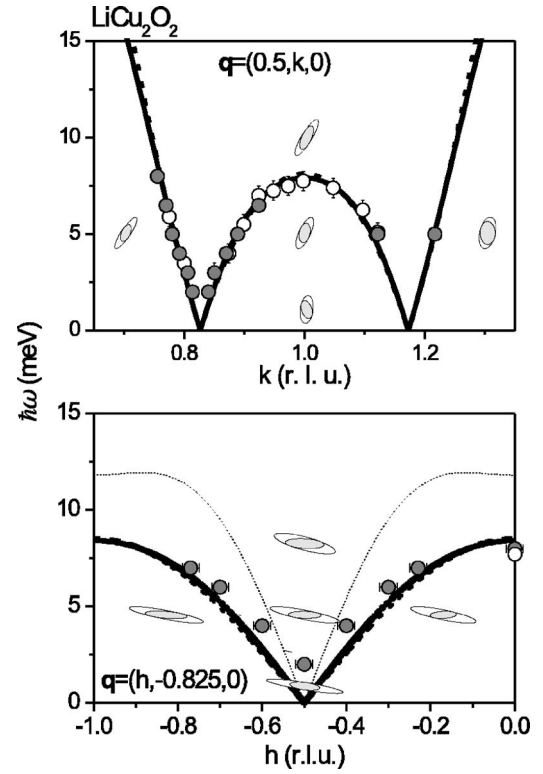


FIG. 4. Spin wave dispersion measured in LiCu_2O_2 at $T=1.5$ K (symbols). Shaded and open circles are data points obtained from constant- E and constant- q scans, respectively. The lines are a fit to the data, as described in the text. Heavy solid, heavy dashed, and thin dotted lines correspond to Models 1, 2, and 3, respectively. In both panels the ellipses represent the FWHM of the instrument resolution function in the appropriate projection (open ellipse) and section (shaded ellipse).

2–15 meV and found to be fully consistent with that shown in Fig. 5(c).

A. Data analysis

In order to extract the relevant exchange constants from the measured dispersion curves the data were analyzed in the framework of semiclassical spin wave theory (SWT).¹³

1. Equivalent Bravais lattice

In LiCu_2O_2 there are four magnetic ions per unit cell. However, within the approximation Hamiltonian (1), any interactions between the double-chain layers are ignored, and the spin lattice becomes topologically a Bravais one. The transformation to a spatial Bravais lattice is made by displacing the atoms as shown in Fig. 1(b). The dynamic structure factor $S_0(\mathbf{q}, \omega)$ of this “straightened out” spin network is directly related to that of the original model through

$$S(\mathbf{q}, \omega) = S_0(\mathbf{q}, \omega) \cos^2 \frac{\mathbf{q}\mathbf{d}}{2} + S_0(\mathbf{q} + (0, 1, 0), \omega) \sin^2 \frac{\mathbf{q}\mathbf{d}}{2}, \quad (2a)$$

$$\mathbf{q}\mathbf{d} = 2\pi h\delta_x + 2\pi l\delta_z, \quad (2b)$$

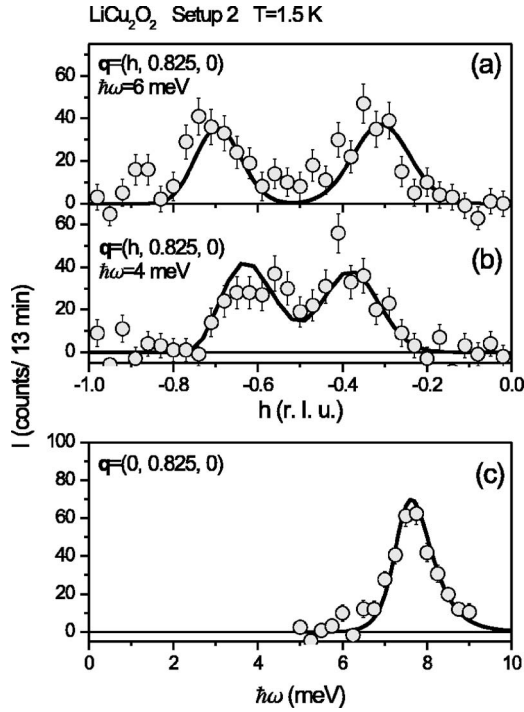


FIG. 5. Typical scans measured in LiCu_2O_2 using Setup 2 (symbols). The lines are as in Fig. 2.

where $\mathbf{q}=(h,k,l)$ is the wave vector transfer and \mathbf{d} is the relative displacement of the two legs in each double chain: $\mathbf{d}=\mathbf{a}\delta_x+\mathbf{c}\delta_z$. For the crystal structure of LiCu_2O_2 we have $\delta_x=0.24$ and $\delta_z=0.19$. It is important to emphasize that Eq. (2) is *exact*: It does not imply any particular properties of $S^{(0)}(\mathbf{q},\omega)$ and $S(\mathbf{q},\omega)$, and relies *only* on the definitions of these correlation functions. While it is possible to derive the excitation energies in the the general (non-Bravais) case, the use of Eq. (2a) is fully valid for our model and greatly facilitates the identification of individual spin wave branches in LiCu_2O_2 .

2. SWT dynamic structure factor

A very useful recipe for calculating the SWT dynamic structure factor can be found in Ref. 14. The magnon dispersion relation is given by:

$$\omega_{\mathbf{q}}^2 = A_{\mathbf{q}}^2 - B_{\mathbf{q}}^2, \quad (3a)$$

$$A_{\mathbf{q}} = 2S \left\{ \frac{J_{\mathbf{q}}}{2} + \frac{1}{4} [J_{\mathbf{q}-\mathbf{q}_0} + J_{\mathbf{q}+\mathbf{q}_0}] - J_{\mathbf{q}_0} \right\}, \quad (3b)$$

$$B_{\mathbf{q}} = 2S \left\{ \frac{J_{\mathbf{q}}}{2} - \frac{1}{4} [J_{\mathbf{q}-\mathbf{q}_0} + J_{\mathbf{q}+\mathbf{q}_0}] \right\}, \quad (3c)$$

where, for our model Hamiltonian

$$J_{h,k,l} = 2J_1 \cos(\pi k) + 2J_2 \cos(2\pi k) + 2J_4 \cos(4\pi k) + 2J_{\perp} \cos(2\pi h). \quad (4)$$

The requirement that \mathbf{q}_0 minimizes $J(\mathbf{q})$ fixes the relation between J_1, J_2, J_4 , and ζ

$$J_1 + 4J_2 \cos(\pi\zeta) + 16J_4 \cos(\pi\zeta)\cos(2\pi\zeta) = 0. \quad (5)$$

Conveniently, J_{\perp} does not enter this expression. The single-magnon cross section has three contributions

$$S_0^{\perp}(\mathbf{q},\omega) = \frac{SA_{\mathbf{q}} + B_{\mathbf{q}}}{2ga_{\mathbf{q}}} \delta(\omega - \omega_{\mathbf{q}}), \quad (6a)$$

$$S_0^{-}(\mathbf{q},\omega) = \frac{SA_{\mathbf{q}-\mathbf{q}_0} - B_{\mathbf{q}-\mathbf{q}_0}}{8\omega_{\mathbf{q}-\mathbf{q}_0}} \delta(\omega - \omega_{\mathbf{q}-\mathbf{q}_0}), \quad (6b)$$

$$S_0^{+}(\mathbf{q},\omega) = \frac{SA_{\mathbf{q}+\mathbf{q}_0} - B_{\mathbf{q}+\mathbf{q}_0}}{8\omega_{\mathbf{q}+\mathbf{q}_0}} \delta(\omega - \omega_{\mathbf{q}+\mathbf{q}_0}). \quad (6c)$$

Here $S^{\perp}(\mathbf{q},\omega)$ represents fluctuations of the spin component perpendicular to the plane of the helix, while $S^{+}(\mathbf{q},\omega)$ and $S^{-}(\mathbf{q},\omega)$ are in-plane excitations. The total SWT cross section for LiCu_2O_2 is related to $S_0(\mathbf{q},\omega)$ through Eq. (2).

It now becomes clear why measuring spin waves in LiCu_2O_2 is so technically challenging: There are six spin wave branches in each crystallographic domain. As a result, in any experiment one has to deal with a total of 12 spin wave branches, all of which are acoustic and therefore contribute to scattering at low energies. Also, compared to a simple antiferromagnet on a Bravais lattice, the scattering by each individual branch is typically much weaker, since intensity is effectively redistributed between twelve modes. The existence of a suitable, albeit narrow, measurement window that was exploited in our experiments is a fortunate coincidence.

B. Fits to experimental data

The energy of the spin wave branch observed in our experiments clearly goes to zero at the principle magnetic Bragg peaks of the A-type domain. It must therefore be associated with the $S^{\perp}(\mathbf{q},\omega)$ mode and the first term in Eq. (2a). An analysis of the polarization of spin wave excitations is beyond the scope of this work. Nevertheless, we can point out that (a,b) being the spin rotation plane⁶ is consistent with a strong $S^{\perp}(\mathbf{q},\omega)$. Indeed, the corresponding polarization factor for unpolarized neutrons is a maximum for in-plane momentum transfers.¹⁴ As a first step in our analysis we ignored all other spin wave branches and used Eq. (3a) to fit the experimental data. It is easy to show that there are exactly two sets of exchange parameters that *exactly* reproduce (i) the experimentally determined incommensurability parameter ζ , (ii) the excitation energies at the zone boundaries $(0.5, 1, 0)$ and $(0, 0.827, 0)$, and (iii) the spin wave velocity along the b^* direction near the magnetic Bragg peaks. Using these two sets of parameters as initial points, we employed a least-squares algorithm to best-fit the data under the rigid constraint set by Eq. (5). The two resulting optimized sets of parameters are listed in Table I and will be referred to as Models 1 and 2, respectively. For a purpose that will be made clear in the next section, we also attempted a fit to the

TABLE I. Sets of exchange constants obtained by fitting the calculated spin wave dispersion relation to the experimental curves in comparison with first-principle calculations.^a

	Model 1 (meV)	Model 2 (meV)	Model 3	LDA ^b (meV)
J_1	3.2 (0.5)	52.8 (4.0)	0 (fixed)	0.4
J_2^c	-5.95	16.9	-7.0 meV	-8.1
J_4	3.7 (0.3)	-0.8 (0.1)	3.75 (0.05) meV	14.4
J_\perp	0.9 (0.1)	0.12 (0.01)	3.4 (0.2) meV	5.7

^aNote the difference in the definition of J compared to Ref. 8.

^bFrom Ref. 7.

^cNot refined: fixed by Eq. (5).

data taken *only along the b axis* while fixing $J_1 \equiv 0$. The measured *a*-axis dispersion was not included in this fit. The resulting set of exchange constants is also listed in Table I and will be referred to as Model 3. Dispersion relations for the out-of-plane branch and the first term in Eq. (2a) calculated for type-A domains using Models 1 through 3 are plotted in lines in Fig. 4.

The next step is to understand why the other 11 spin wave branches were not observed in the studied wave vector and energy ranges. All 12 dispersion curves calculated using Model 1 are plotted in Fig. 6(a). The intensities of each branch were scaled by the energy transfer [to get rid of the $1/\omega$ factors in Eq. (6)] and are plotted in Fig. 6(b). The neutron polarization factor was not included in this calculation, and the maximum value (unity) was assumed for each branch. One readily sees that all branches originating from type-B domains and the first term in Eq. (2a) are extremely weak in our area of interest. The same is true for all spin waves associated with type-A domains and the second term in Eq. (2a). Contributions from type-B domains and the second term in Eq. (2a) are either weak or at very high energy. In the end, only the “principal” modes originating from type-A domains and the first term in Eq. (2a) are relevant to our experiments. Of these three branches the two in-plane modes are almost entirely outside the studied energy range and do not affect any of the scans collected. As a result, only one out-of-plane mode is seen. Similar arguments can be made regarding the dispersion measured along the *a* axis. The simulation also explains why we were unable to follow the “principal” out-of-plane mode to higher energies. At around 8 meV energy transfer any inelastic scans become crowded with a host of peaks associated with other spin wave branches that can not be reliably resolved due to limited experimental resolution.

From Fig. 4 it is apparent that the studied energy and wave vector transfer range the dispersion relations produced by Model 2 are virtually identical to those resulting from Model 1. Both models fit the available experimental data rather well. The only small discrepancy is seen along the *a* direction where the observed spin wave velocity near $\mathbf{q} = (-0.5, 0.827, 0)$ appears slightly larger than calculated, while the zone-boundary energy at $\mathbf{q} = (0, 0.827, 0)$ is slightly smaller. This discrepancy is easily explained if one assumes a small anisotropy-induced gap Δ in the spin wave spectrum

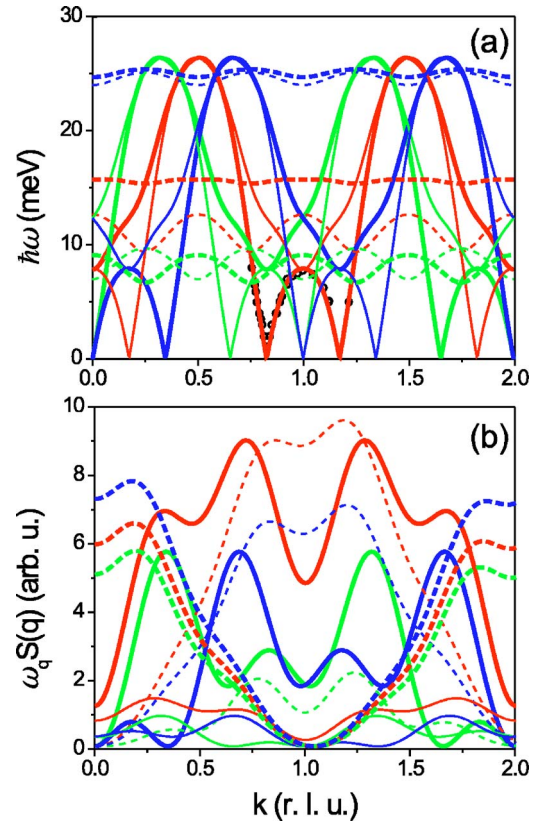


FIG. 6. (Color online) (a) Dispersion of all 12 spin wave branches along the $(0.5, k, 0)$ reciprocal-space rod in twinned LiCu₂O₂ crystals calculated using Model 1. (b) The corresponding structure factors scaled by energy transfer. In both panels the out-of-plane modes are plotted in red. Modes shown in blue and green lines are polarized in the plane of spin rotation. Thick and thin lines of all types correspond to the first and second terms in Eq. (2a), respectively. Solid and dashed lines refer to type-A and type-B crystallographic domains. Symbols are as in the top panel of Fig. 4.

at the magnetic Bragg peak position. From the existing scans it is possible to tentatively estimate $\Delta \approx 1.5$ meV, though more high-resolution data will be needed for a reliable determination. As far as only the *b*-axis dispersion is concerned, Model 3 seems to work just as well as the other two sets of parameters, and for the $(0.5, k, 0)$ reciprocal-space rod produces almost identical curves. However, this good agreement under the constraint $J_1 = 0$ necessarily results in a very poor agreement with the *a*-axis dispersion relation. The corresponding bandwidth calculated using Model 3 [thin dotted line in Fig. 4(b)] is considerably larger than the observed value. In other words, assuming $J_1 = 0$ in Hamiltonian (1) can not be made consistent with the bulk of the experimental data.

The resulting parameter values for Model 1 were used to simulate the measured inelastic neutron scans. For this purpose we utilized the magnetic dynamic structure factor as given by Eq. (6a). This model cross section was scaled by the magnetic form factor for Cu²⁺ and numerically convoluted with the four-dimensional spectrometer resolution function. The latter was calculated in Gaussian form using the Cooper-Nathans approximation. The evolution of the cor-

responding FWHM resolution ellipsoid in the surveyed areas of (E, \mathbf{q}) space is shown in Fig. 4. An overall scaling factor was chosen to best fit the measured scans. The results of such simulations are shown in solid lines in Figs. 2–5. Overall, the experimental peak shapes are well explained by resolution effects alone.

IV. DISCUSSION

As mentioned in the Introduction, the knowledge of spin wave dispersion in an ordered magnetic material can, in principle, provide comprehensive information on the exchange interactions. This requires measurements of dispersion curves across the entire Brillouin zone. In the particular case of LiCu_2O_2 , twinning, less than perfect sample mosaic, and a complex spectrum limit us to only observing spin waves in the direct proximity of the principal magnetic Bragg reflections. For this reason the resulting sets of parameters can be regarded as unique only under the assumption of the validity of Hamiltonian (1) and the SWT approximation.

The Hamiltonian has a solid justification in the crystal structure, and is well supported by first-principles calculations. However, a vital question is to what extent an analysis based on essentially classical spin wave theory can be valid in the case of a quasi-low-dimensional frustrated magnet such as LiCu_2O_2 ? At the very least, the exchange constants obtained from such an analysis will be renormalized compared to their actual values due to quantum corrections. This is particularly true for interchain interactions, for which SWT exchange parameters are typically much smaller than the actual ones. Nevertheless, even for highly anisotropic or frustrated systems, acoustic modes can be associated with waves in the order parameter field. In this case a *renormalized* SWT with some *effective* set of exchange parameters typically works rather well. Just two examples are the weakly coupled $S=1/2$ chains compound KCuF_3 (Ref. 15) and the quasi-2D frustrated helimagnet Cs_2CuCl_4 .¹⁴ Deviations from classical behavior in LiCu_2O_2 do not appear particularly severe. The typical energy scale of exchange interactions computed by local density approximation (LDA) exceeds the temperature of three-dimensional (3D) long-range ordering by less than an order of magnitude. While the absolute value of the ordered moment has not been determined to date, that in the very similar helimagnet NaCu_2O_2 is quite large ($0.64 \mu_B$).¹² We therefore have good reason to assume that *renormalized* SWT will work well for our system.

Turning now to the two solutions that were obtained, we note that Model 2 almost exactly corresponds to the simple J_1 - J_2 model that we originally proposed.⁶ However, unless the renormalization of exchange constants is severe, their large values appear unrealistic. Indeed, these parameters are an order of magnitude larger than those estimated by fitting the measured magnetic susceptibility to the J_1 - J_2 model.⁶ In addition, a straightforward estimate of the Curie-Weiss temperature $T_{C-W} = 2S(S+1)J(0)/(3k_B) = (J_1 + J_2 + J_4 + J_\perp)/k_B$ for Model 2 yields $T_{C-W} \sim 800$ K. This value is vastly greater than the actual $T_{C-W} = 40$ K,¹⁶ as estimated from the susceptibility data of Ref. 6.

We thus conclude that Model 1 is much more likely to be an adequate description of LiCu_2O_2 . Considering that the SWT exchange constants are renormalized compared to their actual values, the predicted $T_{C-W} \sim 21$ K is consistent with experimental observation. Additional support for Model 1 could be potentially found in measurements of the dispersion relation along the c axis, that were not performed in the present study. However, since there are no obvious dominant interlayer exchange pathways in the LiCu_2O_2 structure, an analysis of c -axis dispersion would necessarily introduce several small interlayer exchange parameters. This, in turn, would result in an over-parametrized problem and would not necessarily help to unambiguously establish J_1 , J_2 , and J_4 .

The key features of Model 1, namely, a *ferromagnetic* J_2 bond and a substantial J_4 coupling constant, are similar to those of the LDA calculations of Ref. 7. The mechanism of geometric frustration in LiCu_2O_2 is thus similar to that in NaCu_2O_2 .¹² The main difference between the exchange parameters in Model 1 and those emerging from LDA calculations of Ref. 7 is in the magnitude of J_1 . As illustrated by Model 3, assuming that J_1 is negligibly small makes the SWT calculation incompatible with the measurements. We conclude that either LDA severely underestimate J_1 , or this exchange constant is renormalized by an order of magnitude in the SWT. Of course, one can never entirely rule out the possibility that both the LDA calculations and our SWT analysis are missing some crucial terms in the Hamiltonian. Further experimental and theoretical insight will be required to fully resolve this remaining inconsistency.

V. CONCLUSION

In summary, based on inelastic neutron scattering measurements we can conclude that the simple J_1 - J_2 model that we originally proposed does not apply to LiCu_2O_2 . The frustration mechanism is more complex and resembles that proposed in Refs. 7 and 11. It involves a competition between a combination of antiferromagnetic J_1 and ferromagnetic J_2 interactions against an additional antiferromagnetic long-range J_4 coupling. We find the three corresponding exchange constants to be of comparable absolute strength. This discrepancy between a SWT-based interpretation of the experimental data and first-principles calculations remains to be explained.

ACKNOWLEDGMENTS

One of the authors (A.Z.) would like to thank A. Drechsler for numerous insightful discussions on the subject and for his constructive comments (Ref. 11) on Ref. 6. This work was partially supported by the Civilian Research and Development Foundation Project No. RU-P1-2599-04. Work at ORNL was carried out under Contract No. DE-AC05-00OR22725, U.S. Department of Energy. Part of this work was done at the Swiss Neutron Spallation Source SINQ, Switzerland.

- ¹A. M. Vorotynov, A. I. Pankrats, G. A. Petrakovkii, K. A. Sablina, W. Paszkowicz, and H. Szymczak, *JETP* **86**, 064424 (1998); *J. Magn. Magn. Mater.* **188**, 233 (1998).
- ²F. Fritschij, H. Brom, and R. Berger, *Solid State Commun.* **107**, 719 (1998).
- ³S. Zvyagin, G. Cao, Y. Xin, S. McCall, T. Caldwell, W. Moulton, L.-C. Brunel, A. Angerhofer, and J. E. Crow, *Phys. Rev. B* **66**, 064424 (2002).
- ⁴D. A. Zatsopin, V. R. Galakhov, M. A. Korotin, V. V. Fedorenko, E. Z. Kurmaev, S. Rartkowski, M. Neumann, and R. Berger, *Phys. Rev. B* **57**, 4377 (1998).
- ⁵B. Roessli, U. Staub, A. Amato, D. Herlach, P. Pattison, K. Sablina, and G. A. Petrakovskii, *Physica B* **296**, 306 (2001).
- ⁶T. Masuda, A. Zheludev, A. Bush, M. Markina, and A. Vasiliev, *Phys. Rev. Lett.* **92**, 177201 (2004).
- ⁷A. A. Gippius, E. N. Morozova, A. S. Moskvin, A. V. Zalessky, A. A. Bush, M. Baenitz, H. Rosner, and S.-L. Drechsler, *Phys. Rev. B* **70**, 020406 (2004).
- ⁸T. Masuda, A. Zheludev, A. Bush, M. Markina, and A. Vasiliev, *Phys. Rev. Lett.* **94**, 039706 (2005). Note: There is a factor of two difference in the definition of exchange constants relative to the present work and to Ref. 7. The discrepancy is due to the definition of J in the Hamiltonian, where each bond is counted twice, as opposed to the convention used in this work, where each bond enters the sum once only.
- ⁹C. K. Majumdar and D. K. Ghosh, *J. Math. Phys.* **10**, 1388 (1969); B. S. Shastry and B. Sutherland, *Phys. Rev. Lett.* **47**, 964 (1981); F. D. M. Haldane, *Phys. Rev. B* **25**, 4925 (1982); S. R. White and I. Affleck, *ibid.* **54**, 9862 (1996); A. A. Aligia, C. D. Batista, and F. H. L. Essler, *ibid.* **62**, 3259 (2000) and references therein.
- ¹⁰T. Tonegawa and I. Harada, *J. Phys. Soc. Jpn.* **56**, 2153 (1987); R. Chitra, Swapan Pati, H. R. Krishnamurthy, Diptiman Sen, and S. Ramasesha, *Phys. Rev. B* **52**, 6581 (1995).
- ¹¹S.-L. Drechsler, J. Mlek, J. Richter, A. S. Moskvin, A. A. Gippius, and H. Rosner, *Phys. Rev. Lett.* **94**, 039705 (2005).
- ¹²L. Capogna, M. Mayr, P. Horsch, M. Raichle, R. K. Kremer, M. Sofin, A. Maljuk, M. Jansen, and B. Keimer, cond-mat/0411753 (unpublished).
- ¹³See, for example, T. Nagamiya, *Solid State Physics* (Academic Press, New York, 1967), Vol. 20, p. 305.
- ¹⁴R. Coldea, D. A. Tennant, and Z. Tylczynski, *Phys. Rev. B* **68**, 134424 (2003).
- ¹⁵D. A. Tennant, S. Nagler, D. Welz, G. Shirane, and K. Yamada, *Phys. Rev. B* **52**, 13381 (1995).
- ¹⁶In Ref. 3 T_{C-W} is cited as 80 K. As discussed in Ref. 6, this discrepancy is due to the contamination of the samples used in Ref. 3 with the Li_2CuO_2 phase. This impurity phase also produces a sharp peak in susceptibility at $T=9$ K that is absent in our samples.